

Probing R -parity violating models of neutrino mass at the LHC via top squark decays

Amitava Datta^{(a)1} and Sujoy Poddar^{(a)2}

^(a) *Indian Institute of Science Education and Research, Kolkata,
HC-VII, Sector III, Salt Lake City, Kolkata 700 106, India.*

Abstract

It is shown that the R -parity violating decays of the lighter top squarks (\tilde{t}_1) triggered by the lepton number violating couplings λ'_{i33} , where the lepton family index $i = 1-3$, can be observed at the LHC via the dilepton di-jet channel even if the coupling is as small as 10^{-4} or 10^{-5} , which is the case in several models of neutrino mass, provided it is the next lightest supersymmetric particle(NLSP) the lightest neutralino being the lightest supersymmetric particle(LSP). We have first obtained a fairly model independent estimate of the minimum observable value of the parameter ($P_{ij} \equiv BR(\tilde{t} \rightarrow l_i^+ b) \times BR(\tilde{t}^* \rightarrow l_j^- \bar{b})$) at the LHC for an integrated luminosity of 10fb^{-1} as a function of $m_{\tilde{t}_1}$ by a standard Pythia based analysis. We have then computed the parameter P_{ij} in several representative models of neutrino mass constrained by the neutrino oscillation data and have found that the theoretical predictions are above the estimated minimum observable levels for a wide region of the parameter space.

¹adatta@iiserkol.ac.in

²sujoy_phy@iiserkol.ac.in

1 Introduction

Neutrino oscillation experiments[1] have confirmed that neutrinos indeed have very tiny masses, several orders of magnitude smaller than any other fermion mass in the Standard Model (SM). The tiny masses of the neutrinos, however small, provide evidences of new physics beyond the SM.

Neutrinos can be either Dirac fermions or Majorana fermions depending upon whether the theory is lepton number conserving or violating. In the SM, as originally proposed by Glashow, Salam and Weinberg, neutrinos are massless since right handed neutrinos and lepton number violating terms are not included.

Both R -parity conserving (RPC) or R -parity violating (RPV) minimal supersymmetric extension of the SM (MSSM)[2] are attractive examples of physics beyond the SM. In general the MSSM may contain RPC as well as RPV couplings. The latter include both lepton number and baryon number violating terms which result in catastrophic proton decays. One escape route is to impose R -parity as a symmetry which eliminates all RPV couplings. This model is generally referred to as the RPC MSSM. However, neutrino masses can be naturally introduced in this model only if it is embeded in a grand unified theory (GUT) [3]. Tiny Majorana neutrino masses are then generated by the see-saw mechanism [4]. Proton decay is a crucial test for most of the models belonging to this type.

However, an attractive alternative for generating Majorana masses of the neutrinos without allowing proton decay is to impose a discrete symmetry which eliminates baryon number violating couplings from the RPV sector of the MSSM but retains the lepton number violating ones. The observation of neutrinoless double beta decay[5] and absence of proton decay may be the hallmark of such RPV models of neutrino mass.

The GUT based models though very elegant have hardly any unambiguous prediction which may tested at the large hadron collider(LHC). In contrast the RPV models of neutrino mass are based on TeV scale physics and, consequently, have many novel collider signatures.

The observables in the neutrino sector not only depend on the RPV parameters but also on the RPC ones like the masses of the superpartners generically called sparticles. Thus the precise determination of the neutrino masses and mixing angles in neutrino oscillation experiments together with the measurement of sparticle masses and branching ratios (BRs) at collider experiments can indeed test the viability of the RPV models quantitatively. Moreover the collider signatures of this model are quite distinct from that of the RPC model. In this

paper our focus will be on a novel signature of a RPV model of ν mass which can be easily probed at the early stages of the upcoming LHC experiments.

In the RPC models the lightest supersymmetric particle (LSP) decays into lepton number violating channels producing signals with high multiplicity but without much missing energy which are in sharp contrast with the signals in a typical RPC model. In RPV MSSM the sparticles other than the LSP can also directly decay via lepton number violating channels which may lead to spectacular collider signatures. However, in a typical model of neutrino mass consistent with the oscillation data such couplings turn out to be so small[6] that the RPC decay of the sparticles overwhelm the RPV decays. Thus the LSP decay is the only signature of R -parity violation.

However, the scenario changes dramatically if we consider the direct RPV decay of the lighter top squark (\tilde{t}_1) [7, 8, 9, 10] with the assumption that \tilde{t}_1 it is the next lightest supersymmetric particle(NLSP) while the lightest neutralino ($\tilde{\chi}_1^0$) is the LSP. The theoretical motivation for the \tilde{t}_1 -NLSP scenario is the fact that it's superpartner - the top quark- is much heavier than any other matter particle in SM. This large top mass (m_t) leads to a spectacular mixing effect in the top squark mass matrix which suppresses the mass of the lighter eigenstate [2]. We assume that \tilde{t}_1 -NLSP decays via the loop induced mode $\tilde{t}_1 \rightarrow c\tilde{\chi}_1^0$ [11] and the four body[12] decay mode, which occurs only in higher order of perturbation theory, with significant BR. The validity of this assumption will be justified later. The RPV decays can now naturally compete with the RPC ones in spite of the fact that couplings underlying the former modes are highly suppressed by the ν oscillation data [13].

The lighter top squark decays into a lepton and a b -jet via RPV couplings λ'_{i33} are listed below:

$$a) \tilde{t}_1 \rightarrow l_i^+ b ; \quad b) \tilde{t}_1^* \rightarrow l_i^- \bar{b} \quad (1)$$

where $i=1-3$ corresponds to e , μ and τ respectively. Our signal consists of opposite sign dileptons(OSDL), two hard jets with very little \cancel{E}_T . These modes dominate, e.g., in many RPV models where neutrino masses are generated at the one loop level by the λ'_{i33} couplings, where i is the lepton index and 3 stands for quarks or squarks belonging to the third generation (see below).

We take the lowest order QCD cross section of top squark pair production which depends on $m_{\tilde{t}_1}$ only. Requiring that the significance of the signal over the SM background be at least 5σ level for an integrated luminosity of $10 fb^{-1}$ or smaller, we can then put fairly model

independent lower limits on the products of the BRs (PBRs) of the RPV decay modes in Eq. 1. In our analysis both the signal and the backgrounds are simulated with Pythia. As expected the range of $m_{\tilde{t}_1}$ which can be probed at the LHC is significantly larger compared to the reach of Tevatron RUN II[14, 15]. The details of our simulations will be presented in the next section.

In principle the viability of probing any RPV model of neutrino mass with the above characteristics at the LHC can be checked by computing PBRs in respective models, and comparing with the estimated lower limits. For the purpose of illustration we have considered in section 3 a model based on three bilinear RPV couplings (μ_i) and three trilinear couplings (λ'_{i33}) at the weak scale [16] and have carried out the above check. It is gratifying to note that most of the parameter space allowed by the neutrino oscillation data can be probed by the early LHC experiments with an integrated luminosity of 10 fb^{-1} (see section 3). Moreover, the constraints from oscillation data indicate that the λ'_{i33} couplings should have certain hierarchical pattern leading to distinct collider signatures [17]. This hierarchy among the couplings can be qualitatively tested by observing the relative sizes of signals involving different OSDL signals.

The summary, the conclusions and future outlooks are in the last section.

2 The signals and the SM backgrounds

The production and decay of the lighter top squark pairs are simulated by Pythia[18]. Initial and final state radiation, decay, hadronization, fragmentation and jet formation are implemented following the standard procedures in Pythia. We have considered only the RPV decay modes of \tilde{t}_1 via the couplings λ'_{i33} , $i = 1-3$ (Eq. 1) and in this section their BRs are taken to be free parameters. We have used the toy calorimeter simulation (PYCELL) in Pythia with the following criteria:

- The calorimeter coverage is $|\eta| < 4.5$. The segmentation is given by $\Delta\eta \times \Delta\phi = 0.09 \times 0.09$ which resembles a generic LHC detector.
- A cone algorithm with $\Delta R(j, j) = \sqrt{\Delta\eta^2 + \Delta\phi^2} = 0.5$ has been used for jet finding.
- Jets are ordered in E_T and $E_{T,\min}^{\text{jet}} = 30\text{GeV}$.

Various combinations of OSLDs in the final state are selected as follows:

- Only tau leptons decaying into hadrons are selected provided the resulting jet has $P_T \geq 30$ GeV and $|\eta| < 3.0$.
- Leptons ($l = e, \mu$) are selected with $P_T \geq 20$ GeV and $|\eta| < 2.5$.

The following selection criteria(SC) are used for background rejection :

- The τ -jets are tagged according to the tagging efficiencies provided by the CMS collaboration[19](Fig. 12.9)(SC1). Hadronic BR of the τ is also included in the corresponding efficiency. For e and μ SC1 is the lepton-jet isolation cut. We require $\Delta R(l, j) > 0.5$. The detection efficiency of the leptons are assumed to be approximately 100% for simplicity.
- Events with two isolated leptonic objects (e, μ or tagged τ -jets) are rejected if $P_T \leq 150$ GeV, where $l = e$ or μ (SC2) or $E_T^{V(\tau)} < 100$ GeV, where $E_T^{V(\tau)}$ is the E_T of the τ jet.
- We select events with exactly two jets other than the tagged τ -jets (SC3). The event is rejected if the additional jets have $P_T \leq 100$ GeV (SC 4).³
- Events with missing transverse energy (\cancel{E}_T) > 60 GeV are rejected (SC5).

Through SC1 we have severely constrained the transverse momentum of two leptons $l = e, \mu$ to reject the leptons coming from the leptonic decays of the tau. Moreover such a strong cut reduces most of the SM backgrounds significantly. We have considered backgrounds from: $WW, WZ, ZZ, t\bar{t}$, Drell-Yan (DY) and QCD events. The missing energy veto plays a crucial role to tame down WW and $t\bar{t}$ backgrounds as they are rich in missing energy. Mistagging of light jets as τ -jets is a major source of background to di-tau events. We have taken this into account. However, if we also employ b -tagging then this background can be brought under control to some extent.

In our work b tagging has been implemented according to the following prescription. A jet with $|\eta| < 2.5$ matching with a B-hadron of decay length > 0.9 mm has been marked *tagged*. The above criteria ensures that $\epsilon_b \simeq 0.5$ in $t\bar{t}$ events, where ϵ_b is the single b -jet

³It is expected that this cut would also suppress the SUSY backgrounds due to, e.g., \tilde{q}, \tilde{g} production.

tagging efficiency (i.e., the ratio of the number of tagged b -jets and the number of taggable b -jets in $t\bar{t}$ events).

The leading order(LO) cross-sections for $\tilde{t}_1 - \tilde{t}_1^*$ pairs presented in Table 1 are computed using calcHEP (version 2.3.7)[20].

Signal	240	300	400	450	500
$\sigma(pb)$	14.6	4.8	1.1	0.58	0.32

Table 1: $\tilde{t}_1 - \tilde{t}_1^*$ pair production cross section (σ) at the LHC for different $m_{\tilde{t}_1}$.

In Table 2 we have presented the combined efficiencies of SC1 - SC5 in steps. The first column of Table 2 shows signals with different topology of final states. Here eeX , $\tau\tau X$, $e\tau X$ and $e\mu X$ represent final states without b -jet tagging. The cumulative efficiency of each SC for $m_{\tilde{t}_1} = 400$ GeV is presented in the next five columns. However, we have not separately presented the efficiencies corresponding to final states with muons as we have assumed that both e and μ are detected with approximately 100% efficiency.

Table 3 contains the effect of b -jet tagging on different final states. We have used the notations $0b$, $1b$ and $2b$ to specify signal events with zero, one and two tagged b -jets respectively. From this Table it is also evident that the efficiencies increase for larger $m_{\tilde{t}_1}$ since the P_T cut on leptons become less severe. This compensates the fall of the cross section with increasing $m_{\tilde{t}_1}$ to some extent.

$\tilde{t}_1\tilde{t}_1^*$	ϵ_1	ϵ_2	ϵ_3	ϵ_4	ϵ_5
eeX	0.93708	0.292239	0.087228	0.043344	0.032823
$\tau\tau X$	0.251343	0.111546	0.033201	0.031554	0.008955
$e\mu X$	0.94101	0.295239	0.088216	0.043415	0.033060
$e\tau X$	0.474948	0.180945	0.053820	0.044793	0.016965

Table 2: Efficiency table for $m_{\tilde{t}_1} = 400$ GeV.

In Table 4 we have shown the effect of cuts on the background from $t\bar{t}$ events. SC2 is very effective in reducing this background significantly. Moreover this background is accompanied

	SIGNAL				
$m_{\tilde{t}_1} (GeV)$	240	300	400	450	500
$e e 0b$	0.00032	0.00066	0.00189	0.00234	0.00255
$e e 1b$	0.00121	0.00330	0.01116	0.01461	0.01580
$e e 2b$	0.00176	0.00509	0.01984	0.02620	0.03121
$e e X$	0.00328	0.00905	0.03282	0.04315	0.04957
$\tau \tau 0b$	0.00059	0.00073	0.00112	0.00091	0.00097
$\tau \tau 1b$	0.00153	0.00284	0.00363	0.00351	0.00391
$\tau \tau 2b$	0.00126	0.00226	0.00421	0.00450	0.00522
$\tau \tau X$	0.00338	0.00582	0.00896	0.00892	0.01098
$\tau e 0b$	0.00045	0.00081	0.00148	0.00142	0.00142
$\tau e 1b$	0.00135	0.00307	0.00667	0.00705	0.00717
$\tau e 2b$	0.00126	0.00346	0.00882	0.00997	0.01078
$\tau e X$	0.00308	0.00734	0.01697	0.01843	0.01936
$\mu e 0b$	0.000315	0.00067	0.00190	0.00235	0.00257
$\mu e 1b$	0.00123	0.00334	0.01125	0.01469	0.01635
$\mu e 2b$	0.00178	0.00512	0.01992	0.02625	0.03129
$\mu e X$	0.00332	0.00912	0.03306	0.04329	0.05021

Table 3: Final efficiencies for different $m_{\tilde{t}_1}$ (including b-tagging if implemented).

$t\bar{t}$	ϵ_1	ϵ_2	ϵ_3	ϵ_4	ϵ_5
ee	7.63×10^{-3}	2.22×10^{-5}	5.70×10^{-6}	7.00×10^{-7}	1.00×10^{-7}
$\tau\tau$	4.76×10^{-4}	4.00×10^{-6}	1.50×10^{-6}	1.00×10^{-6}	4.00×10^{-7}
$e\mu$	7.74×10^{-3}	2.01×10^{-5}	6.01×10^{-6}	6.80×10^{-7}	5.0×10^{-7}
$e\tau$	1.88×10^{-3}	9.3×10^{-6}	2.95×10^{-5}	9.50×10^{-7}	2.00×10^{-7}

Table 4: Efficiency table for $t\bar{t}$ process

by large amount of \cancel{E}_T and SC5 also reduces it significantly. Since $t\bar{t}$ decays contain two b quarks, b -tagging is not very effective here and has not been included in Table 4.

QCD	ϵ_1	ϵ_2	ϵ_3	ϵ_4	ϵ_5
ee	1.16×10^{-5}	0	0	0	0
$\tau\tau$	9.10×10^{-3}	4.02×10^{-3}	1.05×10^{-3}	2.85×10^{-4}	2.10×10^{-4}
$e\mu$	6.0×10^{-6}	0	0	0	0
$e\tau$	0	0	0	0	0

Table 5: Efficiency table for the QCD process in the \hat{p}_T bin: $400 \text{ GeV} < \hat{p}_T < 1000 \text{ GeV}$.

Table 5 presents another important background arising from the $2 \rightarrow 2$ processes due to pure QCD interactions for $400 \text{ GeV} < \hat{p}_T < 1000 \text{ GeV}$, where \hat{p}_T is the transverse momentum of the two partons in the final state. However, SC2 completely kills all backgrounds except for those with the di- τ final states. The latter background, mainly due to mistagging of light flavour jets as τ -jets, affect the di- τ signal very seriously. The mistagging probability has also been taken from [19] (Fig. 12.9).

This background is very large, as expected, since the QCD cross-section is very large. The leading order cross-sections have been computed by Pythia in two \hat{p}_T bins : (i) $400 \text{ GeV} < \hat{p}_T < 1000 \text{ GeV}$ and (ii) $1000 \text{ GeV} < \hat{p}_T < 2000 \text{ GeV}$. We have chosen the QCD scale to be $\sqrt{\hat{s}}$. The corresponding cross-sections being 2090 pb and 10 pb respectively. Beyond 2000 GeV the number of events are negligible. We shall discuss later how the visibility of the di- τ signal can be improved by employing b tagging.

In Table 6 we have computed the numerically significant backgrounds of all types for $\mathcal{L} = 10 \text{ fb}^{-1}$. Here '-' denotes a vanishingly small background. It is clear from this table that only $t\bar{t}$ and QCD backgrounds are relevant. The LO cross-sections in the second row of Table 6 except for the QCD processes have been computed using calcHEP(version 2.3.7)[20]. Due to very strong cut on P_T of highest two leptons SC2 DY type backgrounds become vanishingly small. Moreover, SC3 and SC4 finally reduce it to zero. Other backgrounds like WW , WZ and ZZ become vanishingly small mainly due to SC2.

The Product Branching Ratio (PBR) is defined as :

$$P_{ij} \equiv BR(\tilde{t}_1 \rightarrow l_i^+ b) \times BR(\tilde{t}_1^* \rightarrow l_j^- \bar{b}) \quad (2)$$

where i or j can run from 1-3 corresponding to e , μ and τ respectively. The Minimum Observable Product Branching Ratio(MOPBR $\equiv P_{ij}^{min}$) corresponds to $S/\sqrt{(B)} \geq 5$, where

	BACKGROUND					
Final state	W^+W^-	$W^\pm Z$	ZZ	$t\bar{t}$	QCD	DY
$\sigma(pb)$	73.5	33.4	10.1	400	2090,10.6	3400
$e e 0b$	0.37	0.33	0.40	0.40	-	-
$e e 1b$	-	-	-	-	-	-
$e e 2b$	-	-	-	-	-	-
$e e$	0.37	0.33	0.40	0.40	-	-
$\tau \tau 0b$	-	-	-	-	4218	-
$\tau \tau 1b$	-	-	-	0.80	143	-
$\tau \tau 2b$	-	-	0.20	0.80	12	-
$\tau \tau$	-	-	0.20	1.60	4373	-
$\tau e 0b$	-	-	-	-	-	-
$\tau e 1b$	-	-	-	0.40	-	-
$\tau e 2b$	-	-	-	0.40	-	-
τe	-	-	-	0.80	-	-
$\mu e 0b$	0.37	-	-	0.40	-	-
$\mu e 1b$	-	-	-	0.80	-	-
$\mu e 2b$	-	-	-	0.80	-	-
μe	0.37	-	-	2.00	-	-

Table 6: Total number of all types of backgrounds survived after all cuts .

S and B are the number of signal and background events respectively. However, for a typical signal with negligible background we have required $S \geq 10$ as the limit of observability and MOPBR is computed accordingly.

For a given \mathcal{L} the MOPBR for each process is computed from Table 3 and Table 6 by following expression:

$$P_{ij}^{min} = \frac{5\sqrt{\eta\mathcal{L}\Sigma\sigma^b\epsilon^b}}{\eta\mathcal{L}\sigma(\tilde{t}_1\tilde{t}_1^*)\epsilon}, \quad (3)$$

where P_{ij} is already defined in Eq. 2. σ^b and ϵ^b (not to be confused with ϵ_b , the b -jet tagging efficiency) denote the cross section and the efficiency of background of type b . Similarly ϵ is the final efficiency for the signal. η is 2 for $i \neq j$ and η is 1 for $i = j$. The integrated luminosity \mathcal{L} is taken to be 10 fb^{-1} . The estimated MOPBRs are given in Table 7 (without b -jet tagging) and Table 8 (with two tagged b -jets).

We remind the reader that in Table 7 and Table 8 a signal is assumed to be observable if $S \geq 10$ even if B is ≤ 4 . In Table 7 and Table 8 a '×' indicates that corresponding channel can not be probed.

Our conclusions so far have been based on LO cross sections. If the next to leading order corrections are included the $\tilde{t}_1 - \tilde{t}_1^*$ production cross section is enhanced by 30 - 40 % due to a K-factor[21]. It is then clear from Eq. 3, that the estimated MOPBR would remain unaltered even if all significant background cross sections are enhanced by a factor of two due to higher order corrections.

$m_{\tilde{t}_1} (GeV)$	240	300	400	450	500
$P_{11}^{min}(\%)$	2.1	2.3	2.8	4.0	6.3
$P_{33}^{min}(\%)$	×	×	×	×	×
$P_{12}^{min}(\%)$	1.0	1.1	1.4	2.0	3.4
$P_{13}^{min}(\%)$	1.1	1.4	2.7	4.7	8.0

Table 7: Minimum value of PBR estimated from the sample without b tagging .

We present in Fig. 1 the distribution (unnormalised) of invariant mass of a electron -jet pair in the dielectron-dijet sample without b -tagging for $m_{\tilde{t}_1} = 300 GeV$. We first reconstruct invariant mass for all possible electron-jet pair. Among these pairs We select the two such that the difference in their invariant mass is minimum. We then plot the higher of the two invariant masses. This peak, if observed, would unambiguously establish the lepton number violating nature of the underlying decay. In contrast if neutralino decay is the only signal of R -parity violation, then this information may not be available. For example, if $\tilde{\chi}_1^0 \rightarrow \nu b\bar{b}$ is

$m_{\tilde{t}_1} (GeV)$	240	300	400	450	500
$P_{11}^{min}(\%)$	3.9	4.1	4.5	6.6	10.0
$P_{33}^{min}(\%)$	9.4	16.0	37.5	66.4	×
$P_{12}^{min}(\%)$	1.9	2.0	2.3	3.3	5.0
$P_{13}^{min}(\%)$	2.7	3.0	5.2	8.6	14.5

Table 8: Minimum value of PBR estimated from the 2- b tagged sample.

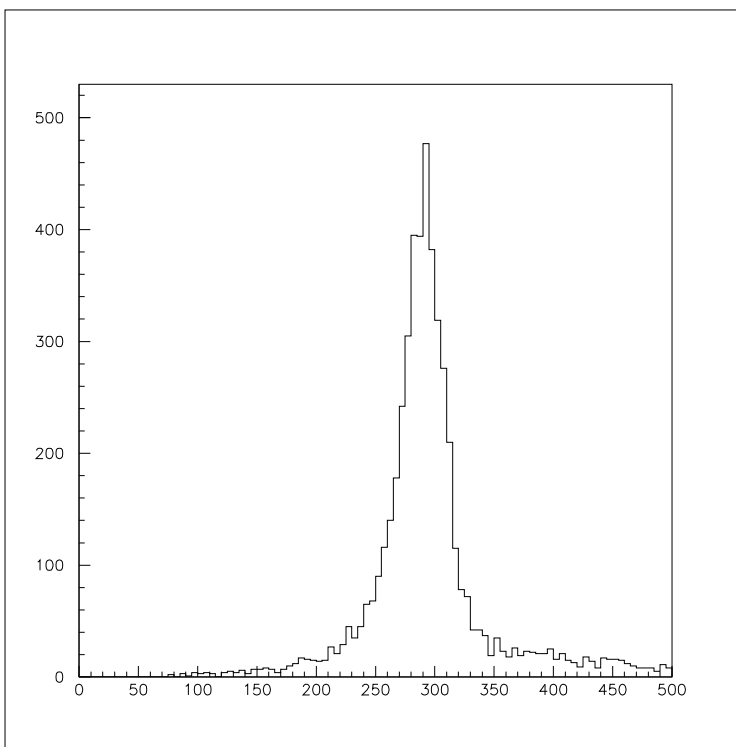


Figure 1: The invariant mass distribution for $m_{\tilde{t}_1} = 300 GeV$.

the dominant decay mode of the LSP via the λ'_{33} coupling then the lepton number violating nature of the decay dynamics will be hard to establish.

In the next section we shall calculate the PBR for different signals in a realistic models of neutrino mass constrained by the neutrino oscillation data and examine whether the predictions exceed the corresponding MOPBR estimated in this section. Our main aim is to illustrate that the LHC experiments will be sufficiently sensitive to probe these models and not to make an exhaustive study of all possible models.

3 Model Calculations

The collider signatures considered in the last section arise only in models with non-vanishing trilinear λ'_{i33} type couplings at the weak scale. However, consistency with neutrino oscillation data require the introduction of more RPV parameters (bilinear superpotential terms, bilinear soft breaking terms etc)[22]. In fact the list of possible choices is quite long. It is expected that the constraints on the λ' couplings in the most general model imposed by the ν - oscillation data will be considerably weaker and the observability of the resulting dilepton-dijet signal will improve. Thus we have restricted ourselves to models with a minimal set of parameters capable of explaining the oscillation data with rather stringent constraints on the λ' couplings.

We work in a basis where the sneutrino vevs are zero. It is assumed that in this basis only three nonzero bilinear(μ_i) and three trilinear(λ'_{i33}) couplings, all defined at the weak scale, are numerically significant. In this framework the neutrino mass matrix receives contributions both at the tree and one loop level. It should be emphasised that the tree level mass matrix, which is independent of λ_{i33} couplings, yields only two massless neutrinos. Thus the interplay of the tree level and one loop mass matrices is essential for consistency with the oscillation data.

The chargino-charge lepton, the neutralino - neutrino and other relevant mixing matrices in this basis may be found in [22]. In principle the diagonalization of these matrices may induce additional lepton number violating couplings which can affect the BRs of the top squark decays considered in this paper. For example, the RPC coupling $\tilde{t}_1 - t - \tilde{W}_3$ may induce new RPV vertices through $\tilde{W}_3 - \nu$ mixing. However, it was shown in[23] that the new modes induced in this way would have negligible BRs. As a result the approximation that the decays of the top squark NLSP are driven by the λ'_{i33} couplings only is justified.

In addition to the RPV parameters the neutrino masses and mixing angles depends on

RPC parameters. In this paper we shall use the following popular assumptions to reduce the number of free parameters in the RPC sector: i) At the weak scale the soft breaking mass squared parameters of the L and R-type squarks belonging to the third generation are assumed to be the same (the other squark masses are not relevant for computing neutrino masses and mixing angles in this model). ii) We shall also use the relation $M_2 \approx 2 M_1$ at the weak scale as is the case in models with a unified gaugino mass at M_G . Here M_1 and M_2 are respectively the soft breaking masses of the U(1) and SU(2) gauginos respectively.

The tree level neutrino mass matrix and, hence, the predicted neutrino masses depends on the parameters of the gaugino sector (through the parameter C [16, 17]). They are M_2 , M_1 , μ (the higgsino mass parameter) and $\tan \beta = v_2/v_1$, where v_1 and v_2 are the vacuum expectation values (vevs) for the down type and the up type neutral higgs bosons respectively. We remind the reader that for relatively large $\tan \beta$ s the loop decay overwhelms the RPV decay [10, 12]. We have, therefore, restricted ourselves to $\tan \beta = 5-8$. It is also convenient to classify various models of the RPC sector according to the relative magnitude of M_2 and μ . If $M_1 < M_2 \ll \mu$, then the lighter chargino ($\tilde{\chi}_1^\pm$), the LSP ($\tilde{\chi}_1^0$) and the second lightest neutralino ($\tilde{\chi}_2^0$) are dominantly gauginos. Such models are referred to as the gaugino-like model. On the other hand in the mixed model ($M_1 < M_2 \approx \mu$), $\tilde{\chi}_1^\pm$ and $\tilde{\chi}_2^0$ are admixtures of gauginos and higgsinos. In both the cases, however, $\tilde{\chi}_1^0$ is purely a bino to a very good approximation. There are models with $M_1, M_2 \gg \mu$ in which $\tilde{\chi}_1^\pm$, $\tilde{\chi}_1^0$ and $\tilde{\chi}_2^0$ are higgsino-like and all have approximately the same mass ($\approx \mu$). It is difficult to accommodate the top squark NLSP in such models without fine adjustments of the parameters. Thus the LSP decay seems to be the only viable collider signature. One can also construct models wino or higgsino dominated LSPs. However, the \tilde{t}_1 -NLSP scenario cannot be naturally accommodated in these frameworks for reasons similar to the one in the last paragraph.

The one loop mass matrix, on the other hand, depends on the sbottom sector (through the parameter K_2 [16, 17]). This parameter decreases for higher values of the common squark mass for the third generation. From the structure of the mass matrix it then appears that for fixed C , identical neutrino masses and mixing angles can be obtained for higher values of the trilinear couplings if K_2 is decreased. Thus at the first sight it seems that arbitrarily large width of the RPV decays may be accommodated for any given neutrino data. This, however, is not correct because of the complicated dependence of the RPV and loop decay BRs of \tilde{t}_1 on the RPC parameters and certain theoretical constraints. The common squark

mass cannot be increased arbitrarily without violating the top squark NLSP condition. Of course larger values of the trilinear soft breaking term A_t may restore the NLSP condition. But larger values of A_t tend to develop a charge colour breaking(CCB) minimum of the scalar potential [24]. Finally the pseudo scalar higgs mass parameter M_A can be increased to satisfy the CCB condition. But as noted earlier [17] that would enhance the loop decay width as well and suppress the BRs of the RPV decay modes.

We have chosen the following RPC scenarios : A) The gaugino dominated model and B)The mixed type model. The choice of RPC parameters for model A) and model B) are: A) $M_1 = 195.0$, $M_2 = 370.0$, $\mu = 710.0$, $\tan\beta = 6.0$, $A_t = 1100.0$, $A_b = 1000.0$, $M_{\tilde{q}}$ (common squark mass)= 450.0 , $M_{\tilde{l}}$ (common slepton mass) = 400.0 and $M_A = 500.0$ and B) $M_1 = 170.0$, $M_2 = 330.0$, $\mu = 320.0$, $\tan\beta = 6.0$, $A_t = 1045.0$, $A_b = 1000.0$, $M_{\tilde{q}}=450.0$, $M_{\tilde{l}} = 400.0$ and $M_A = 200.0$, where all masses and mass parameters are in GeV . Both the scenarios correspond to $m_{\tilde{t}_1} = 240 GeV$ and \tilde{t}_1 is the NLSP. It should be noted that the slepton mass is specified to ensure that the \tilde{t}_1 is the NLSP. It does not affect the neutrino mass matrix.

Even if \tilde{t}_1 is the NLSP the following modes may compete with the RPV decays and overwhelm it:

$$a) \tilde{t}_1 \rightarrow t\tilde{\chi}_1^0; \quad b) \tilde{t}_1 \rightarrow bW\tilde{\chi}_1^0 \quad c)\tilde{t}_1 \rightarrow c\tilde{\chi}_1^0; \quad d) \tilde{t}_1 \rightarrow f\bar{f}b\tilde{\chi}_1^0 \quad (4)$$

In the parameter spaces we have worked with the mode a) is kinematically disallowed. The second mode is highly suppressed if the LSP is Bino dominated as is assumed in this analysis. Thus in the scenario under consideration only modes c) and d) may compete with RPV decays of \tilde{t}_1 . In this section we have computed the PBRs taking into account the competition among the above three modes.

Next we have randomly generated bilinear and trilinear RPV couplings, μ_i and λ'_{i33} . Then these parameters are constrained by ν oscillation data which allows very few sets of RPV parameters for the above RPC parameters. Most of the allowed trilinear RPV couplings lie within $10^{-4} - 10^{-5}$. Finally the relevant PBRs have been calculated in model (A) and (B).

In Table 9 we present several representative sets of trilinear RPV parameters allowed by ν oscillation data and the corresponding PBR. A ‘-’ indicates that the predicted PBR is negligible. As noted before two of the couplings turns out to be large while the third one

is suppressed due to oscillation constraints. It turns out that the PBR's involving the large couplings are larger than the corresponding MOPBRs estimated in the last section even without b-tagging(see Table 7). The only exception is P_{33} which cannot be probed without b-jet tagging (see Table 8)

$\lambda'_{133}[\times 10^{-5}]$	$\lambda'_{233}[\times 10^{-5}]$	$\lambda'_{333}[\times 10^{-5}]$	P_{11}	P_{22}	P_{33}	P_{12}	P_{23}	P_{13}
Model A								
1.6	8.3	10.0	-	5.1	10.8	0.2	7.4	0.3
7.5	0.7	9.2	4.9	-	11.4	-	0.1	7.5
4.6	4.5	0.3	6.8	6.8	-	6.7	-	-
Model B								
11.9	0.99	15.0	4.2	-	10.6	-	-	6.6
0.59	13.6	16.8	-	4.3	10.2	-	6.6	-
7.3	7.4	0.9	6.3	6.6	-	6.4	0.1	0.1

Table 9: Trilinear RPV couplings allowed by ν oscillation data and the corresponding PBRs computed in models A and B (see text) with $m_{\tilde{t}_1} = 240 GeV$.

For larger $m_{\tilde{t}_1}$, there exists allowed RPV parameter space with observable PBRs at the early LHC runs. However, if we go beyond $m_{\tilde{t}_1} = 500 GeV$ the di-tau channel cannot be probed even with b -tagging. Nevertheless, observation of the $e - \tau$ and the $\mu - \tau$ channel will provide evidence for a relatively large λ_{333} . We present in Table 10 for $m_{\tilde{t}_1} = 500 GeV$. The RPC parameters corresponding to a Gaugino model are chosen to be:

$M_1 = 475.0$, $M_2 = 860.0$, $\mu = 1650.0$, $\tan\beta = 6.0$, $A_t = 995.0$, $A_b = 1000.0$, $M_{\tilde{q}}=575.0$, $M_{\tilde{l}} = 525.0$ and $M_A = 300.0$, where all masses and mass parameters are in GeV .

$\lambda'_{133}[\times 10^{-5}]$	$\lambda'_{233}[\times 10^{-5}]$	$\lambda'_{333}[\times 10^{-5}]$	P_{11}	P_{22}	P_{33}	P_{12}	P_{23}	P_{13}
9.1	4.0	6.4	20.7	-	5.1	4.0	2.0	10.3
4.4	10.9	5.6	-	31.4	2.2	5.1	8.3	1.3

Table 10: Same as Table 9 for $m_{\tilde{t}_1} = 500 GeV$.

We have checked that even for $m_{\tilde{t}_1} > 500 \text{ GeV}$ there exists RPV parameter space allowed by oscillation data which leads to observable dilepton -dijet signals in early LHC experiments.

$(\lambda'_{133})^{max}$		$(\lambda'_{233})^{max}$		$(\lambda'_{333})^{max}$	
92		2176		2086	
P_{11}, P_{13}	56	P_{22}, P_{23}	1376	P_{33}, P_{23}	874
P_{11}, P_{12}	15	P_{22}, P_{12}	119	P_{33}, P_{13}	27
P_{11}	2	P_{22}	664	P_{22}, P_{23}	274
P_{12}	10	**	17	P_{11}, P_{13}	25
**	9			P_{23}	45
				P_{33}	304
				**	537

Table 11: Number of allowed solutions in the mixed model($m_{\tilde{t}_1} = 240 \text{ GeV}$) consistent with ν oscillation data which satisfy the MOPBR given in Table 7 and Table 8. The above numbers are estimated for $\mathcal{L} = 10 \text{ fb}^{-1}$.

We have randomly generated 10^9 sets of RPV parameters in the mixed model with $m_{\tilde{t}_1} = 240 \text{ GeV}$. Out of these only 4354 are consistent with the ν -oscillation data. These solutions can be further classified into three groups according to the highest value of λ'_{i33} . The three columns in Table 11 correspond to these groups. The first column in Table 11 contains detailed information about the flavour structure of the RPV couplings in the 92 solutions with the hierarchy $\lambda'_{133} > \lambda'_{233}, \lambda'_{333}$. The next few rows display the number of solutions with predicted PBRs in different channels above the observable limits as given in Table 8. For example, the third row indicates that signals in $ee + 2jets$ and $e\tau + 2jets$ channels are observable with 10 fb^{-1} of data in 56 solutions. These channels, if observed, would further reveal that $\lambda'_{133} > \lambda'_{333} > \lambda'_{233}$. On the other hand observable signals in $ee + 2jets$ and $e\mu + 2jets$ channels as given in the next row would indicate the hierarchy $\lambda'_{133} > \lambda'_{233} > \lambda'_{333}$.

If only one channel, say the $ee + 2jets$, is observed one can conclude that $\lambda'_{133} \gg \lambda'_{233}, \lambda'_{333}$ (see row 5). On the other the observation of the $e\mu + 2jets$ signal only (see row 6) would indicate $\lambda'_{133} \approx \lambda'_{233} \gg \lambda'_{333}$. The channel $e\mu + 2jets$ dominates over the $ee + 2jets$

or the $\mu\mu + 2jets$ channel because of the factor of two which enhances the number of events when leptons of two different flavours with all possible charge combinations are observed. Finally the seventh row with ‘**’ indicates that no signal can be observed with $\mathcal{L} = 10 \text{ fb}^{-1}$

The information in the next two columns are presented following the format and similar inferences about the hierarchy of the λ'_{i33} can be drawn from the lepton flavour content of the final states. We have verified that for $\mathcal{L} = 100\text{fb}^{-1}$ all solutions well predict atleast one P_{ij} above the corresponding P_{ij}^{min} .

4 Conclusion

In conclusion we reiterate that the OSDL signals with same or different flavours of leptons (e, μ or tau-jets) plus two additional jets arising from RPV decays of $\tilde{t}_1 - \tilde{t}_1^*$ pairs produced at the LHC would be a promising channel for probing the RPV coupling λ'_{i33} (see Eq. 1 and the discussions following it). This is true in general if \tilde{t}_1 happens to be the NLSP, which is a theoretically well motivated scenario. This signal is especially interesting in the context of RPV models of neutrino mass. A part of our analysis (section 2), however, is fairly model independent since the size of the signal is necessarily controlled by the production cross section of the $\tilde{t}_1 - \tilde{t}_1^*$ pair as given by QCD and the product branching ratio P_{ij} (see Eq. 2). The model independent estimates of P_{ij}^{min} (see Eq. 3) corresponding to observable signals for different $m_{\tilde{t}_1}$ s (see Eq. 3) for an integrated luminosity of 10 fb^{-1} are presented in Table 7 and Table 8 using the Monte Carlo event generator Pythia. We have optimized the cuts for $m_{\tilde{t}_1} = 240 \text{ GeV}$. However, for even larger values of $m_{\tilde{t}_1}$ the signal efficiencies increase for the same set of cuts keeping the background events almost negligible. Top squark masses in the vicinity of 500 GeV yield observable signals in this channel for realistic models of m_ν . Although our calculations are based on LO top squark pair production cross sections we emphasise that the inclusion of NLO corrections are likely to yield even larger estimates of P_{ij}^{min} as argued in section 2.

We have further noted that inspite of the combinatorial backgrounds, the invariant mass distribution of the lepton (e or μ)-jet pair shows a peak at $m_{\tilde{t}_1}$ (see Fig.1). This peak, if discovered, will clearly establish the lepton number violating nature of the underlying interaction. This may not be possible if neutralino decays happen to be the only RPV signal.

In models of ν -mass, the underlying λ' couplings turn out to be very small. If λ'_{i33} contributes to the one loop ν -mass matrix, it is typically of the order of 10^{-4} - 10^{-5} due to constraints imposed by the ν -oscillation data. Even if λ' is so small the RPV decay of the \tilde{t}_1 -NLSP may have sizable BRs over a large region of the parameter space because the competing loop induced decay (Eq. 4c) or the four body decay (Eq. 4d) of \tilde{t}_1 also have suppressed widths. For the purpose of illustration we have considered a specific model of ν -mass[16] with parameters constrained by the ν -oscillation data. It is interesting to note that in this model most of the theoretically predicted P_{ij} 's (Eq. 2) for several representative choices of RPC parameters turn out to be larger than the P_{ij}^{min} 's estimated in section 2 for $\mathcal{L} = 10 fb^{-1}$. For larger \mathcal{L} almost all solutions yield P_{ij} 's at the observable level. The relative size of the observed final states with various lepton flavour contents will indicate the hierarchy among the λ'_{i33} s for different i 's.

Acknowledgement: AD and SP acknowledge financial support from Department of Science and Technology, Government of India under the project No (SR/S2/HEP-18/2003).

References

- [1] B. T. Cleveland *et al.*, Astrophysical. Jour. **496**, 505 (1998); W. Hampel *et al.* [GALLEX Collaboration], Phys. Lett. B **447**, 127 (1999); M. Apollonio *et al.* [CHOOZ Collaboration], Phys. Lett. B **466**, 415 (1999) Eur. Phys. J. C **27**, 331 (2003); M. Altmann *et al.* [GNO Collaboration], Phys. Lett. B **490**, 16 (2000); Q. R. Ahmad *et al.* [SNO Collaboration], Phys. Rev. Lett. **87**, 071301 (2001), Phys. Rev. Lett. **89**, 011301 (2002), Phys. Rev. Lett. **89**, 011302 (2002); J. N. Abdurashitov *et al.* [SAGE Collaboration]; J. Exp. Theor. Phys. **95** (2002) 181; S. Fukuda *et al.* [Super-Kamiokande Collaboration], Phys. Lett. B **539**, 179 (2002); *ibid*, Phys. Rev. Lett. **89**, 011301 (2002); K. Eguchi *et al.* [KamLAND Collaboration], Phys. Rev. Lett. **90**, 021802 (2003); M.H. Ahn, [K2K Collaboration] Phys. Rev. Lett. **90**, 041801 (2003); M.H. Ahn *etal.*, [K2K Collaboration] Phys. Rev. D **74**, 072003 (2006); P.Adamson *etal.*, [MINOS Collaboration] arxiv:0806.2237[hep-ex].
- [2] For reviews on Supersymmetry, see, *e.g.*, H. P. Nilles, Phys. Rep. **1**, 110 (1984); H. E. Haber and G. Kane, Phys. Rep. **117**, 75 (1985); J. Wess and J. Bagger, *Supersymmetry and Supergravity*, 2nd ed., (Princeton, 1991); M. Drees, P. Roy and

- R. M. Godbole, *Theory and Phenomenology of Sparticles*, (World Scientific, Singapore, 2005).
- [3] For a brief review see, e.g., S. Raby in Review of Particle Physics, Phys. Lett. B **592**, 160 (2004) and references there in.
- [4] M. Gell-Mann, P. Ramond, and R. Slansky, in *Supergravity*, ed. D. Freedman and P. van Nieuwenhuizen (North-Holland, Amsterdam, 1979), p. 315; T. Yanagida, in *Proc. of the Workshop on Unified Theory and Baryon Number in the Universe*, ed. O. Sawada and A. Sugamoto (KEK, Japan, 1979); R. Mohapatra and G. Senjanovic, Phys. Rev. Lett. **44**, 912 (1980), Phys. Rev. D **23**, 165 (1981).
- [5] O.Gemonesi, Int. J. Mod. Phys. A **21**, 1887 (2006); K.Zuber, J. Phys.**G31**, S1471 (2005); S.M.Bilenky, hep-ph/0509098; S.T.Petcov, Phys. Scripta **T121**, 44 (2005); M.Chemtob in [6]; Y.Uchara, Phys. Lett. B **537**, 256 (2002); M.Hirsch, H.V.Klapdor-Kleingrothaus and S.G.Kovalenko, Phys. Rev. D **57**, 1947 (1998), Phys. Rev. Lett. **75**, 17 (1995).
- [6] For reviews on RPV SUSY see, e.g. , H.K. Dreiner, in *Perspectives on Supersymmetry*, ed. G.L. Kane, World Scientific (hep-ph/9707435); A.Barbier *et al.* , Phys. Rep. **420**, 1 (2005) (hep-ph/0406039); M. Chemtob, Prog. Part. Nucl. Phys. **53**, 71 (2005) (hep-ph/04060290).
- [7] Aseshkrishna Datta and B. Mukhopadhyaya,Phys. Rev. Lett. **85**, 248 (2000); D. Restrepo, W. Porod and J. W. F. Valle, Phys. Rev. D **64**, 055011 (2001).
- [8] CDF collaboration (D. Acosta *et al.*), Phys. Rev. Lett. **92**, 051803 (2004).
- [9] S. Chakrabarti, M. Guchait and N. K. Mondal, Phys. Rev. D **68**, 015005 (2003); Phys. Lett. **B600**, 231 (2004).
- [10] S. P. Das, Amitava Datta and M. Guchait, Phys. Rev. D **70**, 015009 (2004).
- [11] K. Hikasa and M. Kobayashi, Phys. Rev. D **36**, 724 (1987).
- [12] C. Boehm, A. Djouadi and Y. Mambrini, Phys. Rev. D **61**, 095006 (2000).
- [13] For neutrino oscillation data, see, e.g. , M.Maltoni *et al.* , New. J. Phys. **6**, 122 (2004).

- [14] T. Aaltonen *et al.* [CDF Collaboration], Phys. Rev. Lett. **101**, 071802 (2008).
- [15] S. P. Das, A. Datta and M. Guchait, Phys. Rev. D **65**, 095006 (2002).
- [16] A. Abada, M. Losada, Phys. Lett. B **492**, 310 (2000).
- [17] S.P.Das, Amitava Datta, S.Poddar, Phys. Rev. D **73**, 075014 (2006).
- [18] T. Sjostrand, P. Eden, C. Friberg, L. Lonnblad, G. Miu, S. Mrenna and E. Norrbin, Comp. Phys. Comm. **135**, 238 (2001), For a more recent version see, (hep-ph/0603175).
- [19] CMS physics, Technical Design Report, vol-I.
- [20] See, *e.g.*, A.Pukhov, CalcHEP—a package for evaluation of Feynman diagrams and integration over multi-particle phase space (hep-ph/9908288). For the more recent versions see: <http://www.ifh.de/pukhov/calchep.html>.
- [21] W. Beenakker, M. Kramer, Tilman Plehn and Michael Spira, hep-ph/9810290.
- [22] For a recent review and further references see, *e.g.*, S. Rakshit, Mod. Phys. Lett. **A19**, 2239 (2004).
- [23] Amitava Datta, S.Poddar, Phys. Rev. D **75**, 075013 (2007).
- [24] See *e.g.*, J.M. Frere, D.R.T. Jones and S. Raby, Nucl. Phys. B **222**, 11 (1983); M. Claudson, L.J. Hall and I. Hinchliffe, Nucl. Phys. B **228**, 501 (1983); J.A. Casas, A. Lleyda and C. Muñoz, Nucl. Phys. B **471**, 3 (1996).